Human Molecular Genetics, 2005, Vol. 14, No. 22 **3523–3538**
doi:10.1093/hmg/ddi381
Advance Access published on October 5, 2005

Abnormal development of the apical ectodermal ridge and polysyndactyly in Megf7-deficient mice

Eric B. Johnson[1], Robert E. Hammer[2] and Joachim Herz[1,*]

[1]Department of Molecular Genetics and [2]Department of Biochemistry, UT Southwestern Medical Center, 5323 Harry Hines Blvd., Dallas, TX 75390-9046, USA

Received July 17, 2005; Revised and Accepted October 3, 2005

***Megf*7/*Lrp*4 is a member of the functionally diverse low-density lipoprotein receptor gene family, a class of ancient and highly conserved cell surface receptors with broad functions in cargo transport and cellular signaling. To gain insight into the as yet unknown biological role of *Megf*7/*Lrp*4, we have disrupted the gene in mice. Homozygous *Megf*7-deficient mice are growth-retarded, with fully penetrant polysyndactyly in their fore and hind limbs, and partially penetrant abnormalities of tooth development. The reason for this developmental abnormality is apparent as early as embryonic day 9.5 when the apical ectodermal ridge (AER), the principal site of *Megf*7 expression at the distal edge of the embryonic limb bud, forms abnormally in the absence of *Megf*7. Ectopic expression and aberrant signaling of several molecules involved in limb patterning, including *Fgf*8, *Shh*, *Bmp*2, *Bmp*4 and *Wnt7a*, as well as the Wnt- and Bmp-responsive transcription factors *Lmx1b* and *Msx*1, result in reduced apoptosis and symmetrical dorsal and ventral expansions of the AER. Abnormal signaling from the AER precedes ectopic chondrocyte condensation and subsequent fusion and duplication of digits in the *Megf*7 knockouts. *Megf*7 can antagonize canonical Wnt signaling *in vitro*. Taken together, these findings are consistent with a role of *Megf*7 as a modulator of cellular signaling pathways involving Wnts, Bmps, Fgfs and Shh. A similar autosomal recessive defect may also occur in man, where polysyndactyly, in combination with craniofacial abnormalities, is also part of a common genetic syndrome.**

INTRODUCTION

*Megf*7/*Lrp*4 (1) belongs to an ancient and highly conserved class of cell surface receptors of which the low-density lipoprotein (LDL) receptor is both the prototype and perhaps the most widely known member (2). Although cargo transport and internalization of macromolecules from the cell surface are the biological functions that are most commonly associated with the LDL receptor gene family, other roles as direct signal transducers or modulators of a broad range of cellular signaling pathways have recently begun to emerge. For instance, the ApoE receptor-2 (*Apoer*2/*Lrp*8) and the very-low-density lipoprotein receptor (*Vldlr*) not only control neuronal migration during brain development (3), but also synaptic transmission in the mature brain (4). LRP1 is one of the most multifunctional members of the family (5) being involved, e.g. in lipoprotein transport, the regulation of cell surface protease activity and the modulation of platelet-derived growth factor receptor-β (PDGFRβ) signaling in the smooth muscle cells of the vascular wall (6–9).

In contrast, the biological functions of *Megf*7/*Lrp*4 have so far remained obscure. In size and structural complexity, it assumes an intermediate place, between the smaller LDL receptor, Apoer2 and Vldlr on one side and the much larger LRP1, LRP1b and megalin on the other (reviewed in 2). Like all other members of the family, it possesses an NPxY sequence in its cytoplasmic domain, a tetraamino acid motif that has been shown to mediate the coupling of these receptors to both, the endocytic machinery (10,11) and to a wide range of intracellular signaling cascades (reviewed in 12). The structural organization of the extracellular domain of *Megf*7 closely resembles that of *Lrp*5 and *Lrp*6, two members of a subfamily of LDL receptor-related proteins (LRPs) that function as co-receptors in the Wnt signaling cascade (13–15).

To gain a first insight into the biological functions of *Megf*7/*Lrp*4, we have knocked out the gene in mice.

*To whom correspondence should be addressed. Tel: +1 2146485633; Fax: +1 2146488804; Email: joachim.herz@utsouthwestern.edu

The resulting autosomal recessive phenotype includes a fully penetrant form of polysyndactyly and a mild and incompletely penetrant form of craniofacial abnormalities, which are also frequently associated with abnormal limb development in humans. These findings suggest a likely role for *Megf*7/*Lrp*4 as a modulator of the signaling pathways that control limb development in the embryo.

A complex coordinated interplay of several different signaling pathways is required for the proper patterning of the complex structure of the distal limb (reviewed in 16). These include several distinct families of signaling molecules such as fibroblast growth factors (*Fgf*), bone morphogenic proteins (*Bmp*), Wnts (*Wnt*) and sonic hedgehog (*Shh*), as well as transcription factors, for instance, *En*1, *Msx*1 and *Lmx*1*b*. An important structure of the developing limb bud is the apical ectodermal ridge (AER), a band of pseudostratified epithelium that arises from the ectoderm and that marks the border between the dorsal and the ventral sides. Proper maintenance of this dorsoventral border is required for the integrity of the AER (17). The AER secretes several of the factors mentioned above and is required for the coordination of growth and patterning, primarily of the distal portions of the limb bud. Bmp receptor 1A, Fgf and Wnt proteins are particularly important for the formation and maintenance of the AER (16,18,19). Deregulated Wnt signaling, caused by a hypomorphic mutation of the negative regulator of Wnt signaling, Dickkopf-1 (*Dkk*1), results in the expansion of the AER, the formation of a doubleridge and a mild form of polysyndactyly (20,21). *Doubleridge* genetically interacts with *En*1 and *Wnt*7*a*, resulting in a more severe and a milder phenotype, respectively (21), and emphasizing the importance of tightly regulated Wnt signaling during limb development. Consistent with these findings, ectodermal Wnt3 signaling is required for the formation and maintenance of the AER (18) and constitutive activation of the canonical Wnt pathway in the limb ectoderm results in the expansion of the AER (19). Likewise, *Bmp receptor 1A*, which mediates Bmp2 and Bmp4 signaling (22), is also required for AER formation (19), as well as for tooth development (23) where it functions upstream of Wnt/β-catenin signaling.

In this study, we have determined that *Megf*7 is expressed in a polarized pattern in the AER and in the ventral ectoderm. Disruption of *Megf*7 results in reduced cell death in the apical ectoderm, symmetrical dorsal and ventral expansion and thickening of the AER, and the abnormal expression of several signaling molecules and transcription factors in a pattern that closely resembles that seen in the *doubleridge* (*Dkk*1$^{d/d}$) mutation. *Megf*7 potently suppresses canonical Wnt signaling in cultured cells. Taken together, these findings suggest that *Megf*7 may function as a negative regulator of Wnt signaling during limb development, although these data do not exclude a larger role as a multifunctional modulator of additional signaling pathways, possibly involving *Fgfs* and *Bmps*.

RESULTS

Generation of Megf7$^{-/-}$ mice

Disruption of *Megf*7 by homologous recombination in embryonic stem cells was achieved by introducing a stop codon just upstream of the transmembrane segment (Fig. 1B). This strategy was chosen, because it prevents the production of a membrane-anchored receptor and eliminates any possibility of any residual functional activity through alternative splicing of the extracellular domain or the use of alternative promoters for transcription initiation. Figure 1A shows the organization of the wild-type and targeted alleles and the location of the DNA probe used for Southern analysis. A stop codon was introduced by site-specific mutation into exon 36 at the 3′ end of the long arm of the targeting vector as described in Materials and Methods. Homologous recombination at the *Megf*7 locus replaces part of exon 36 and 2.1 kb of intron 36 with a PGK*neobpA* expression cassette.

Successful recombination was ascertained by Southern blotting of two independently derived ES cell clones using the indicated probe (Fig. 1C, recombined allele at 4.5 kb) and by PCR (see Materials and Methods). Two independent ES cell clones that were injected into C57Bl/6 blastocysts generated chimeras that sired heterozygous offspring. Both independently derived lines yielded identical results. Homozygous *Megf*7 knockout mice were identified among the live offspring from heterozygous matings at significantly lower than expected ratios using the χ^2 test (27 knockouts out of 169 pups alive at P5, $P < 0.05$), but not among the embryos used for the described *in situ* hybridization studies (99 heterozygotes:100 homozygotes from heterozygote × homozygote matings). Body weight and postnatal growth of homozygous pups were also significantly reduced when compared with wild-type and heterozygous littermates (Fig. 1D). The complete lack of functional transcripts in the knockouts was ascertained by RT–PCR and sequencing of recombinant transcripts (Supplementary Material, Fig. S1).

Polysyndactyly in *Megf*7$^{-/-}$ mice

Homozygous *Megf*7 knockout mice present with polysyndactyly (Fig. 2A), a fully penetrant phenotype that is characterized by the fusion and duplication of digits at both the fore (F) and hind (H) limbs. No other gross abnormalities of axial skeleton or organ systems were noted in the *Megf*7-deficient mice (data not shown). Figure 2B shows Alcian Blue and Alizarin Red staining of adult skeletized fore (F) and hind (H) limbs, revealing extensive bone fusion as well as the presence of extra digits in the knockout (right panels). Mild craniofacial abnormalities, mainly in the form of incisor defects, were found less frequently (Fig. 2C). Sectioning of front and hind paws of 14-day-old wild-type and mutant mice revealed fused digital bones and tendons, club-shaped deformities of digital tips and metaphyseal defects (Supplementary Material, Fig. S2).

To further explore the structural abnormalities of the limb in the *Megf*7-deficient homozygotes, we analyzed the pattern of cartilage formation at different developmental time points (Fig. 3). Whole mount *in situ* hybridization was used to visualize the expression of *Col*2*a*1, a marker for pre-hypertrophic chondrocytes (24), at E11.5 (Fig. 3A) and E12.5 (Fig. 3B) during development. Although the *Col*2*a*1 pattern in the mutants (right panels) at E11.5 is not significantly different from that of wild-type controls (Fig. 3A),

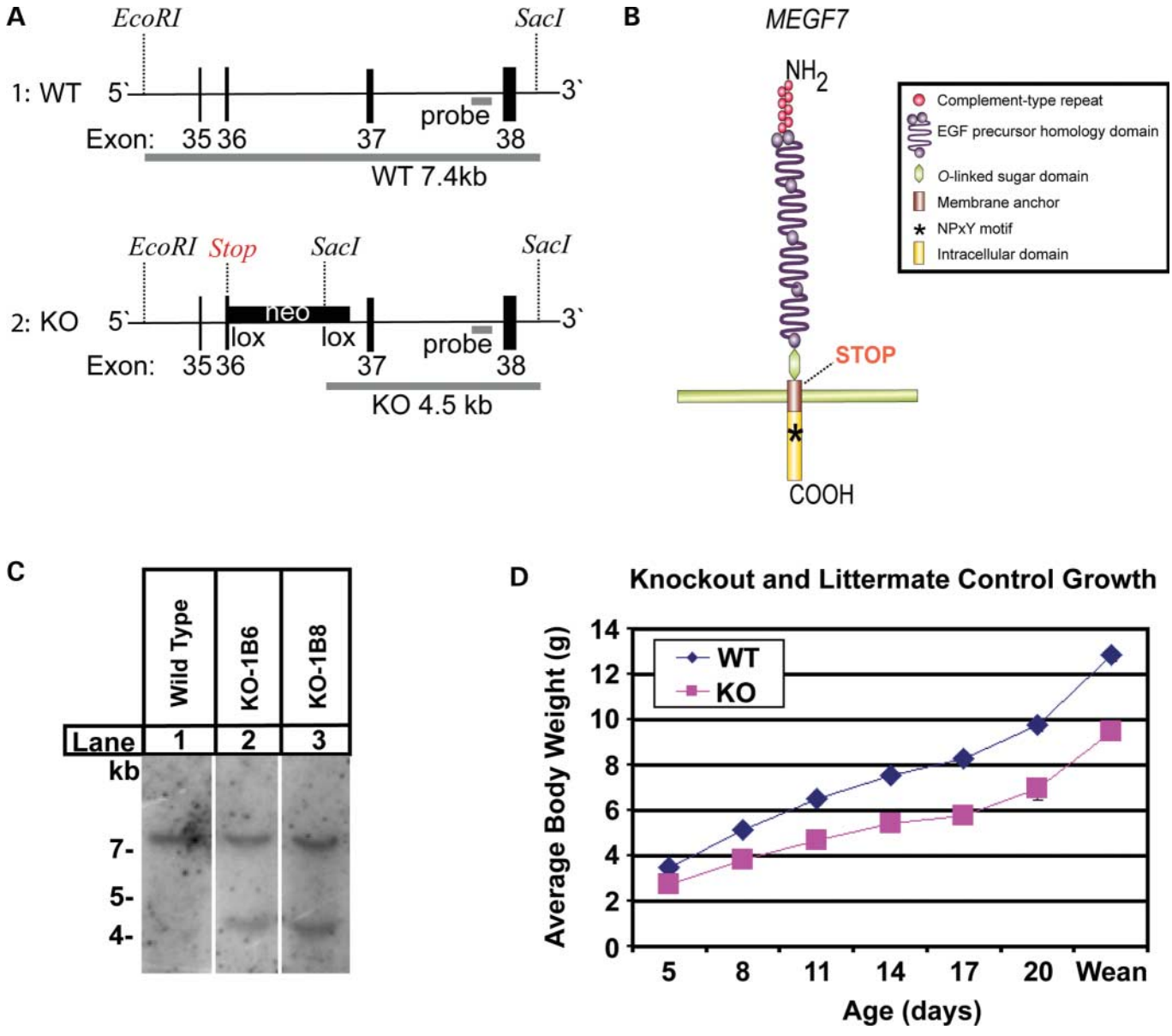

Figure 1. Generation and characterization of *Megf7* knockout mice. (**A**) Structure of wild-type (WT) and mutant (KO) alleles. Wild-type exon 36 was replaced with mutated sequences that introduce a premature *Stop* codon into exon 36 and that delete part of exon 36 and intron 36 in the targeted allele. (**B**) Schematic diagram of the structural domain organization of Megf7 and the location of the *Stop* mutation just amino terminal of the transmembrane segment. (**C**) Southern blot of the ES cell clones used to generate the *Megf7* knockout mice. The wild-type allele yields a 7.4 kb band and the knockout allele yields a 4.5 kb band when genomic DNA is digested with *Eco*RI and *Sac*I and hybridized with the indicated probe. (**D**) Growth curves of wild-type and heterozygous (filled diamonds) and knockout (filled squares) pups from P5 until weaning (P23). Graph indicates average pup weight ± SEM. Error bars fall within the symbols. $P < 0.05$ for all time points.

abnormal chondrocyte compaction and digital fusion is readily apparent in knockout fore (F) and hind (H) limbs at E12.5 (Fig. 3B). Thus, the skeletal defects become manifest between E11.5 and E12.5 of embryonic development. Alcian Blue and Alizarin Red were also used to stain for cartilage and bone in knockout P0 pups (Fig. 3C). As expected from the results obtained in the adults (Fig. 2B), the digital cartilage is broadly fused and calcification of the bones is significantly delayed when compared with the wild-type (left panel).

Megf7 is expressed in the AER

To better understand how Megf7 controls limb development, we examined its developmental expression pattern using whole mount *in situ* hybridization (Fig. 4). *Megf7* transcript was detected in a weak and diffuse pattern in the forelimb bud where it begins to compact at the apical ridge at E9.5 (Fig. 4A, arrows). By E10.5, *Megf7* expression is clearly visible in both the fore (F) and hind (H) limb buds, where it is now restricted to the AER (Fig. 4B, arrows). No signal

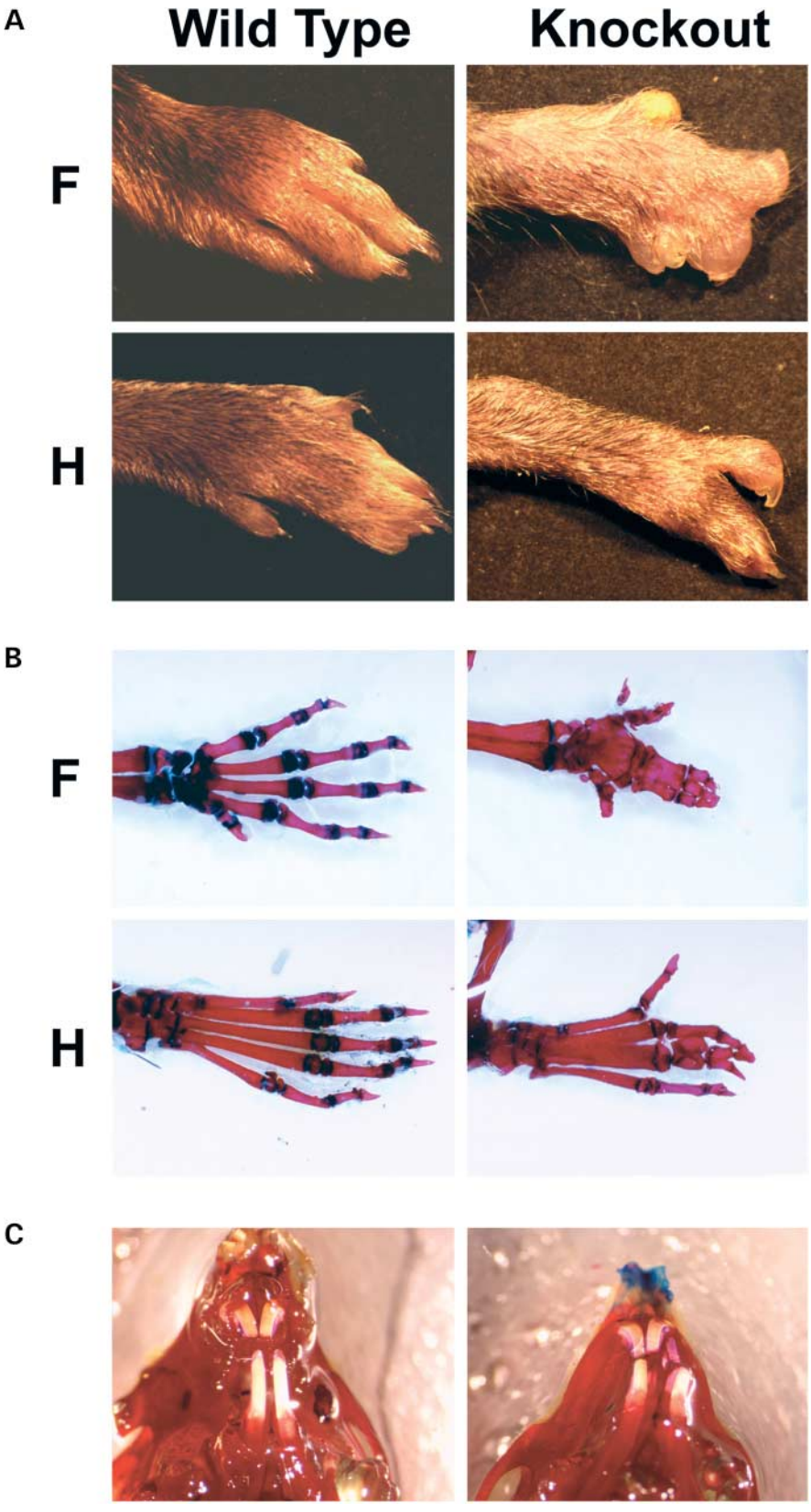

Figure 2. Polysyndactyly in adult *Megf*7 knockout mice. (**A**) Forelimbs (F) and hindlimbs (H) of wild-type (top) and knockout (bottom) adult mice. Duplication and fusion of digits is apparent in the mutants (right panels). (**B**) Alcian Blue and Alizarin Red staining of the autopod of wild-type and knockout fore (F) and hind (H) limbs. Alcian Blue stains cartilage and Alizarin Red stains bone. (**C**) Abnormal tooth development is apparent in some *Megf*7 knockouts.

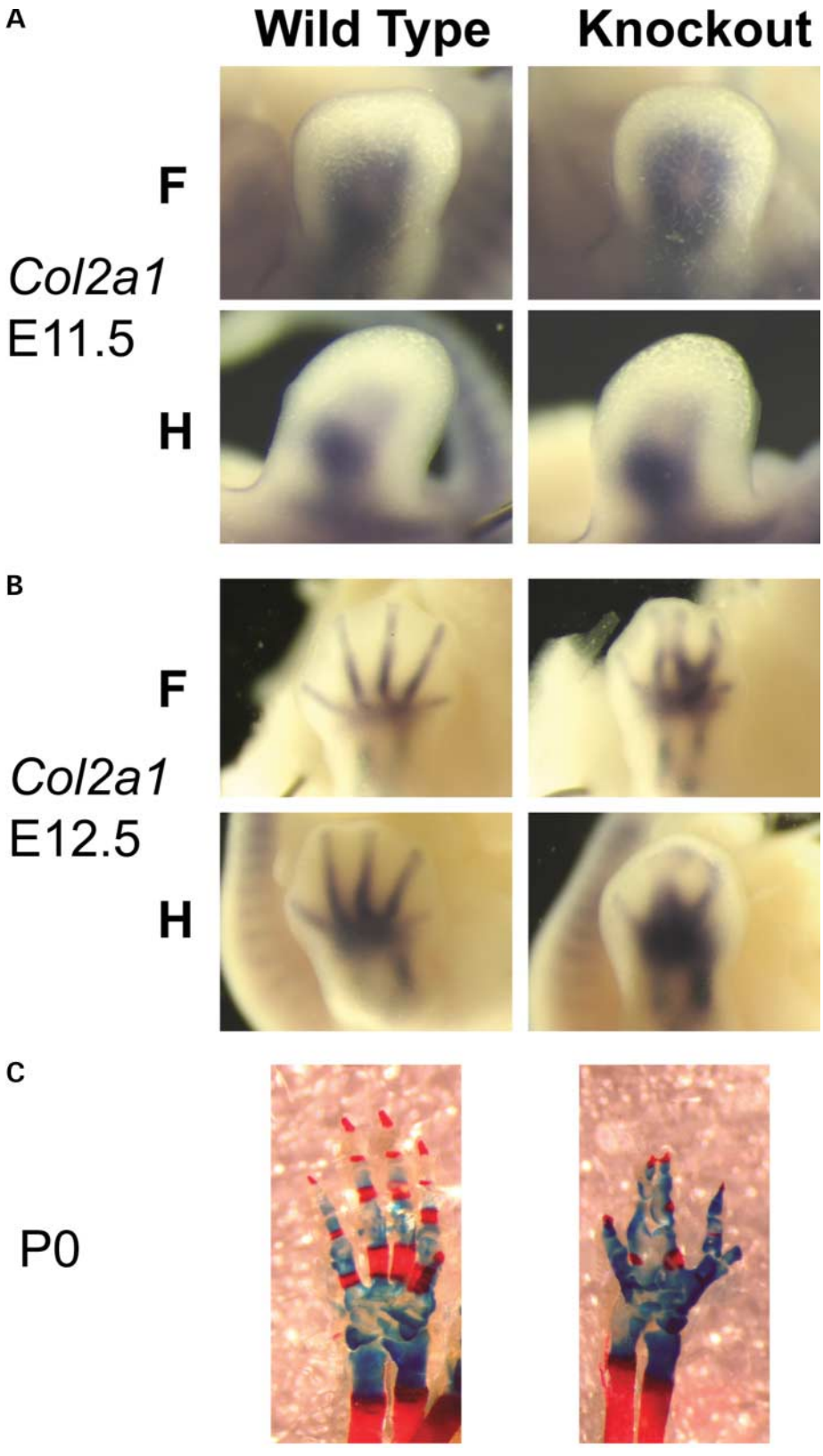

Figure 3. Cartilage development in E11.5 and E12.5 embryonic and P0 newborn mice. (**A**) Whole mount *in situ* hybridization for Col2a1 in E11.5 embryos. Col2a1 staining is similar in wild-type and knockout embryos. (**B**) Whole mount *in situ* hybridization for Col2a1 in E12.5 embryos. Col2a1 staining at E12.5 reveals a defect in chondrocyte condensation in the *Megf*7 knockout that manifests itself between E11.5 and E12.5. (**C**) Alcian Blue and Alizarin Red staining of the autopod of wild-type and knockout limbs at P0. Note fused cartilage and reduced calcification in the knockout.

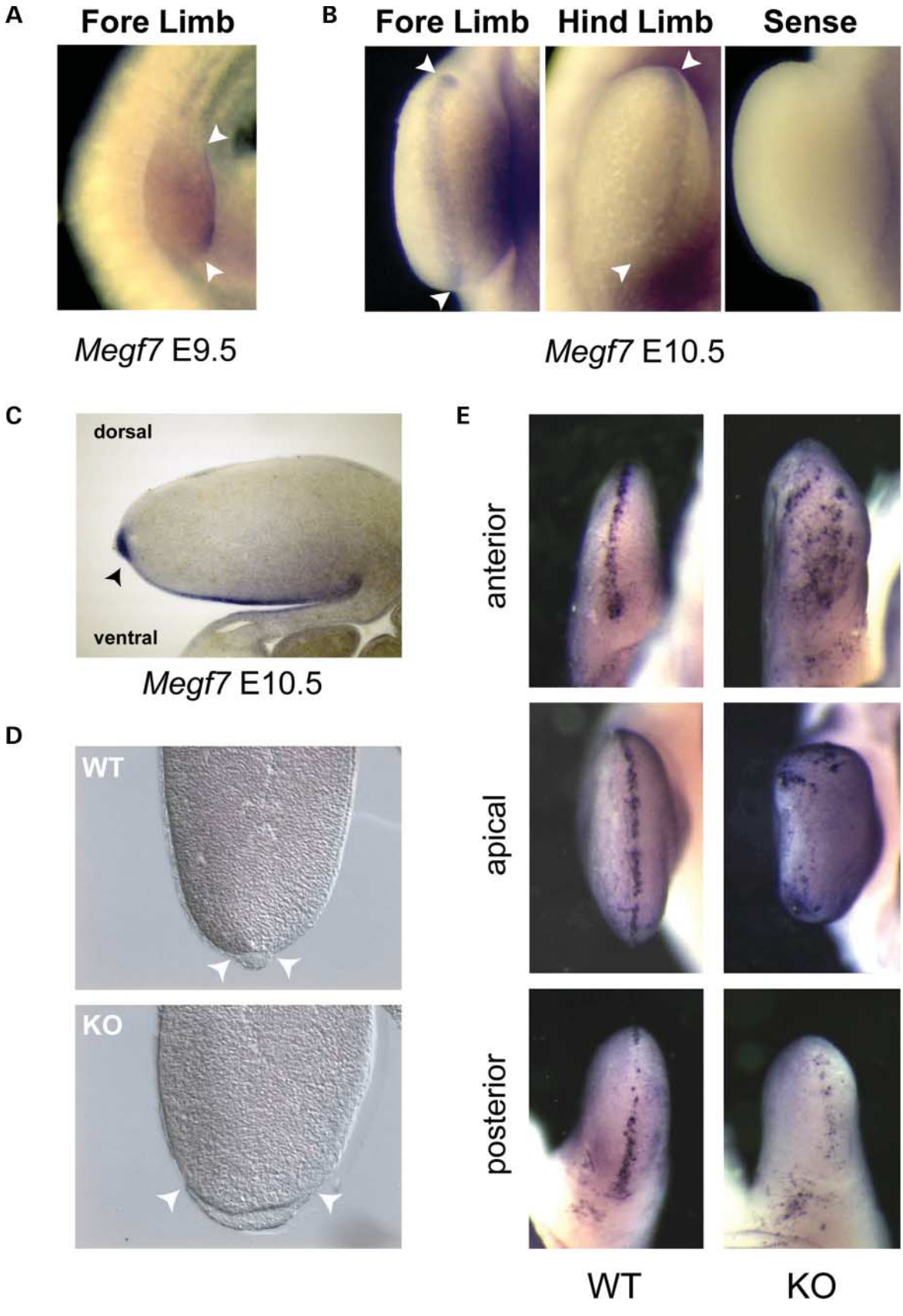
A
Fore Limb
B
Fore Limb
Hind Limb
Sense
Megf7 E9.5
Megf7 E10.5
C
dorsal
ventral
Megf7 E10.5
D
WT
KO
E
anterior
apical
posterior
WT
KO

was observed with a sense probe at any time (right panel, Fig. 4B). Cross-sectioning of E10.5 limb buds revealed strong *Megf*7 expression in the AER and in the ventral ectoderm (Fig. 4C). This highly polarized expression of *Megf*7 is similar to that of *En*1 (32) and suggests that *Megf*7 might be required either for the development of the AER, for the expression of factors that are normally secreted by the AER, or for the normal propagation of signals required for limb development. Under Nomarski optics, the AER in the mutant limb buds was grossly enlarged and broadened compared with wild-type controls (Fig. 4D). To determine whether this might be caused by defects in the execution of the normal apoptotic program in the apical ectoderm, we performed a TUNEL analysis of the developing limbs (Fig. 4E). Apoptotic cells at the surface of the limb bud are normally confined to the AER (WT, left panels), but were virtually absent from the apical section of the knockout AER, and reduced or scattered in the posterior and anterior portions of the AER in the mutant limb buds.

The AER is defective in *Megf*7$^{-/-}$

To further explore this striking defect of the AER, we next used whole mount *in situ* hybridization to investigate the expression pattern of genes that play pivotal roles during limb development. We began by examining the expression pattern of *Fgf*8, which is highly expressed in the AER (16) where it is induced by canonical Wnt signaling (19) and also required for the formation of this structure (Fig. 5). Whole mount *in situ* hybridization shows diffuse expression of *Fgf*8 at E9.5 (Fig. 5A) compared with the wild-type (left panel) that is spread over the entire distal end of the developing limb bud in the *Megf*7 mutants (right panel). Thus, the defect in *Fgf*8 expression caused by disruption of *Megf*7 can already be seen as early as E9.5, the stage when the forelimb bud begins to emerge from the lateral mesoderm. At E10.5 (Fig. 5B) and E11.5 (Fig. 5C), *Fgf*8 continues to fail to compact in the mutants (right panels) into the single distinctive line that identifies the AER in the wild-type (left panels). Instead, *Fgf*8 expression is split into a dorsal and a ventral ridge of high expression, separated by an area of lower and diffuse expressions. This pattern of *Fgf*8 expression is highly reminiscent of that seen in the *doubleridge* mutant (20). The thickening and symmetrical broadening of the *Fgf*8 expressing AER in the mutants is particularly impressive in a cross-section through the limb bud at its apex (Fig. 5D) and consistent with abnormally elevated levels of Wnt signaling in the AER.

The *Shh* expression pattern is disrupted in *Megf*7$^{-/-}$

Shh is a marker for the zone of polarizing activity (ZPA), another organizing center involved in anterior–posterior patterning during limb development (16,25). As is the case for *Fgf*8, the expression pattern of *Shh* (Fig. 6) in *Megf*7 knockout embryos at E10.5 (Fig. 6A) and E11.5 (Fig. 6B) is strikingly similar to that seen in the *doubleridge* mutant (20). *Shh* expression in the posterior mesoderm is present in a dorsal and a ventral patches, which are clearly separated by the AER in the wild-type (Fig. 6A, arrow, top left panel). In contrast, in the mutants the centers of *Shh* expression are more widely spaced apart due to the disruption of the AER (Fig. 6A, arrow, top right panel), with the dorsal patch consistently expressing higher levels of Shh than the ventral one (notched arrows). Overall expression levels in the ventral patch also appear consistently lower than that in the wild-type. This is consistent with the fact that factors secreted from the AER, such as Fgfs, Wnts and Bmps, are required for maximal Shh expression (26–30).

Dorsal–ventral polarity in *Megf*7$^{-/-}$

The striking similarity of the *Megf*7$^{-/-}$ phenotype with the *doubleridge* mutant prompted us to investigate the expression of *Lmx*1*b*, a homeobox transcription factor and *Wnt*7*a* target gene (Fig. 7). *Lmx*1*b* is exclusively expressed in the dorsal mesoderm where it is induced by Wnt7a, which is secreted from the overlying dorsal ectoderm (25,31). Thus, *Lmx*1*b* is an excellent marker that allows us to visualize the state of dorsal–ventral patterning in the *Megf*7 mutants.

Although the dorsal mesoderm continues to be the preferential site of expression of *Lmx*1*b* in the knockout (E9.5, Fig. 7A), the sharp border that defines the boundary between the dorsal and the ventral parts of the limb bud in the wild-type is not as well defined in the mutants at E10.5 and E11.5 (arrows, Fig. 7B and C). This loss of a discrete border between the dorsal and ventral compartments suggests a possible role for *Megf*7 in defining the boundary between the dorsal and ventral limb buds. To confirm this finding, we also performed whole mount *in situ* hybridizations for *Wnt*7*a*, the upstream regulator of *Lmx*1*b*. The zone of *Wnt*7*a* expression in the dorsal ectoderm is displaced proximally from the distal zone of the bud (the future autopod) by the expansion of the AER (Supplementary Material, Fig. S3). However, *Wnt*7*a* expression remains restricted to the dorsal side, in contrast to *En*1 deficiency where *Wnt*7*a* expression extends to the ventral side (32). *Megf*7 may thus act as a regulator of signaling and gene

Figure 4. Whole mount *in situ* hybridization for *Megf*7 and TUNEL staining of wild-type and knockout embryos. *Megf*7 expression was analyzed in embryos at E9.5 (**A**) and E10.5 (**B**). *Megf*7 is expressed in a tight pattern in the AER in E10.5 embryos and in a more diffuse pattern in the E9.5 limb bud (arrows). The panel on the far right in (B) shows the absence of specific signal with the corresponding *Megf*7 sense probe in an E10.5 embryo. Vibratome cross-section of E10.5 wild-type forelimb bud reveals robust *Megf*7 expression in the AER (**C**, arrow) and in the ventral ectoderm. Nomarski staining was used to visualize the AER, which is grossly enlarged and broadened in *Megf*7 knockout (**D**, KO) forelimb buds compared with wild-type (D, WT) controls. Whole mount TUNEL labeling was used to detect apoptotic cells in E11.5 embryos (**E**). Apoptotic cells are concentrated in the AER in wild-type forelimbs (anterior, apical) and hindlimb (posterior) buds. Fewer apoptotic cells are present along the ridgeline in *Megf*7 knockout buds, particularly at the distal (apical) edge of the developing limb, where the number of apoptotic cells is greatly reduced. The remaining TUNEL positive cells are scattered across the broadened AER in the *Megf*7 knockout.

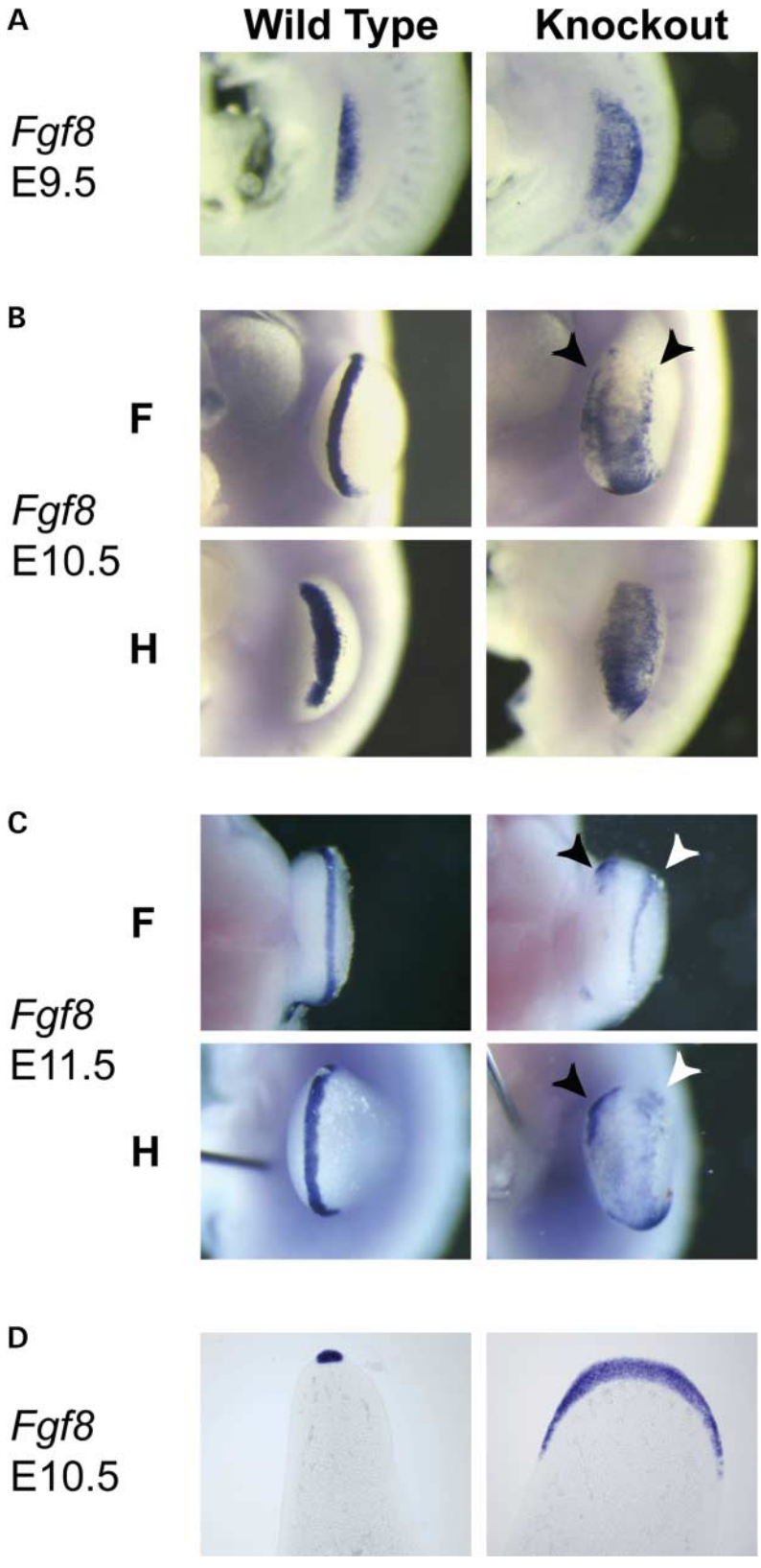

Figure 5. Whole mount *in situ* hybridization for *Fgf*8 in wild-type and knockout embryos. Expression of *Fgf*8 was analyzed in phenotypically wild-type (left panels) and knockout (right panels) embryos at E9.5 (**A**), E10.5 (**B**) and E11.5 (**C**). The AER is disrupted and *Fgf*8 is expressed in a diffuse doubleridged pattern (arrows) at the distal end of the limb bud in knockout embryos. The defect in the expression pattern of *Fgf*8 is apparent as early as E9.5. Vibratome cross-sections of E10.5 forelimb buds show grossly enlarged, *Fgf*8-expressing AER in the knockout (**D**).

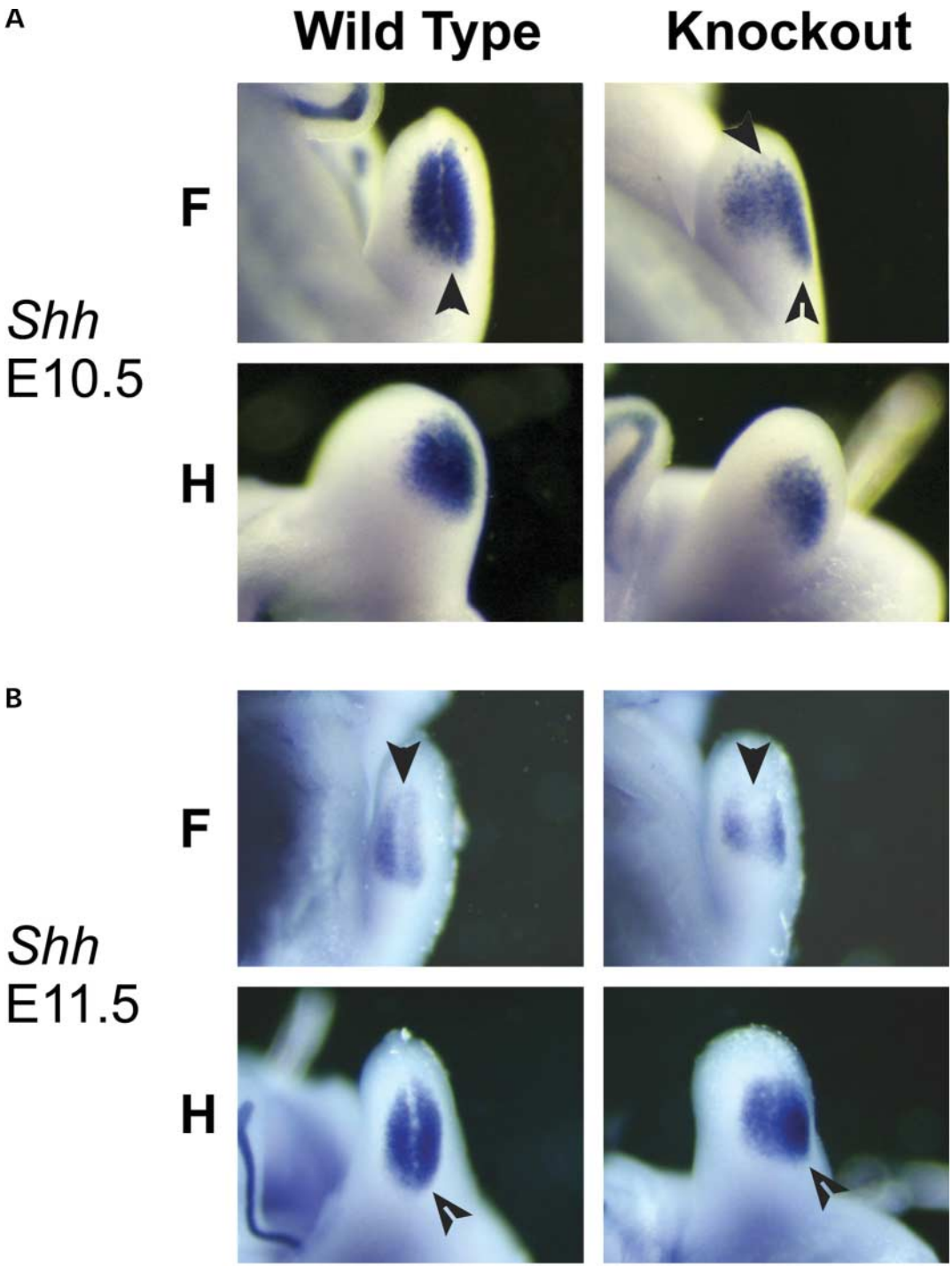

Figure 6. Whole mount *in situ* hybridization for *Shh* in wild-type and knockout embryos. The expression of *Shh* was analyzed in phenotypically wild-type and knockout embryos at E10.5 (**A**) and E11.5 (**B**). Posterior aspects of forelimb (F) and hindlimb (H) buds are shown. *Shh* is expressed in a broadened and more diffuse pattern in the knockout embryos at the posterior distal margin of the limb bud compared with controls. Ventral (left) and dorsal (right) parts of the limb bud are separated by the AER (full arrows). Note relatively higher expression of *Shh* on the dorsal side in the knockout embryos (notched arrows).

expression at the dorsal–ventral border. It is required for the homeostasis of proliferation and apoptosis in the apical ectoderm and may also participate in defining cell identity at the border between the dorsal and ventral compartments of the limb bud.

Abnormal *Bmp* expression in *Megf7*$^{-/-}$

Regulated *Bmp* signaling is important not only for the induction, but also for the maintenance of the AER, and *Bmp*4 is an important factor in the regulation of limb development that is

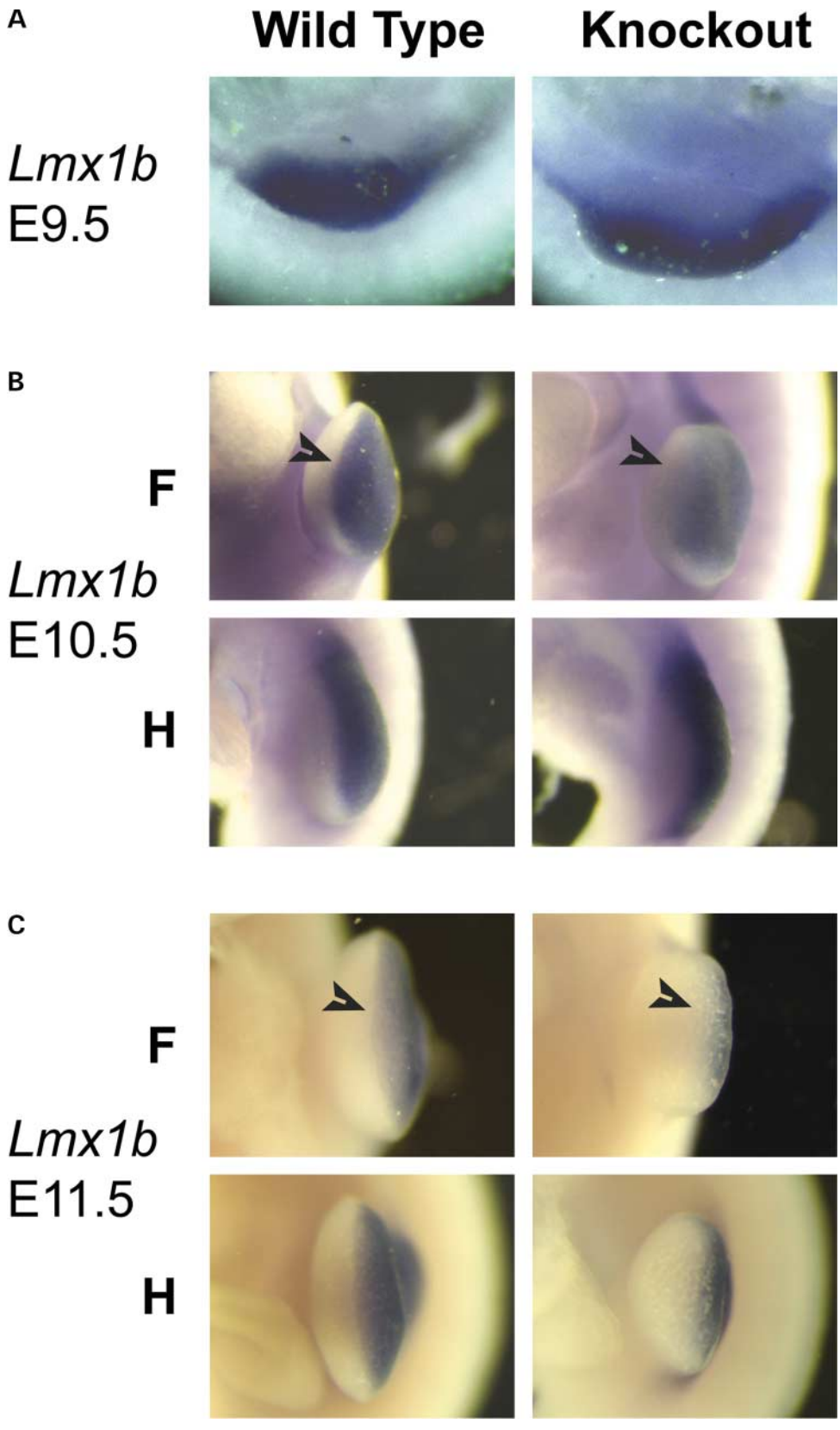

Figure 7. Whole mount *in situ* hybridization for *Lmx1b* in wild-type and knockout embryos. *Lmx1b* expression was analyzed in phenotypically wild-type and knockout embryos at E9.5 (**A**), E10.5 (**B**) and E11.5 (**C**). The sharp dorsal–ventral boundary (arrow, left panel in B and C) is disrupted and diffuse in the knockout (arrow, right panel in B and C) suggesting impaired definition of dorsal and ventral compartments.

secreted from the AER and the underlying mesoderm. It functions upstream of *Shh* to regulate *Shh* expression in the tooth germ and in the developing limb (29,33) and also regulates the expression of *Bmp*2, another Bmp family member that is involved in the specification of digit identity. The expression pattern of *Bmp*4 in the AER mirrors that of *Fgf*8 both in the wild-type and in the *Megf*7 knockout (arrows, Fig. 8A and B), inasmuch as the AER is replaced by a doubleridge, with relatively reduced expression of *Bmp*4 between the medial and lateral ridge lines. As a result, the expression of *Msx*1, a Bmp-responsive gene (28), is both ventrally and dorsally broadened (arrows, Fig. 8C and D).

*Bmp*2 participates in digit specification and its expression is regulated by *Shh* (34). Expression of *Bmp*2 in the *Megf*7 knockout at E11.5 is diffused and the levels do not appear to be significantly different from the wild-type at this stage (Fig. 8E), consistent with the expression of *Shh*, which is still present, albeit at lower levels than in the wild-type (Fig. 6). At E12.5, however, *Bmp*2 expression in the knockout is significantly reduced compared with wild-type embryos and the typical expression pattern of *Bmp*2 in the interdigital mesoderm where *Bmp*2 is involved in the regulation of apoptosis and chondrocyte condensation (35) is disrupted (Fig. 8F).

Hoxd group 11–13 genes are important for the development of the autopod (reviewed in 36). Overall, *Hoxd*12 expression levels in the mutant were comparable to wild-type at E12.5, however, the patterning that is clearly apparent in the wild-type at this stage is lacking in the mutants (Fig. 8G). Similarly, the expression of *Gli*1, a transcription factor that is regulated by *Shh* in the target cell, is disrupted in the mutants and reflects the absence of normal digit specification (Fig. 8H). Taken together, these *in situ* hybridization data reveal the disruption of multiple signaling pathways required for the regulation of normal limb development.

The striking similarity of the *Megf*7 knockout and the *doubleridge* phenotypes, combined with the structural homology of the *Megf*7 extracellular domain with that of the Wnt co-receptors *Lrp*5 and *Lrp*6 (reviewed in 2) prompted us to test, whether *Megf*7, like *Dkk*1, could function as a negative regulator of Wnt signaling. HEK293 cells were transfected using the TOP-Flash Wnt reporter system, in the absence or presence of Wnt1, Megf7, LRP1 or VLDLR, two other members of the LDL receptor gene family. Activation of the canonical (β-catenin) Wnt signaling pathway and subsequent transcription of the firefly luciferase reporter requires the presence of LRP5/6 as well as the interaction of Wnt1 with Frizzled receptors on the surface of the 293 cells. LRP1 has previously been shown to antagonize Wnt signaling by competing with LRP5/6, thereby sequestering Frizzled receptors and disrupting the Wnt signaling complex at the plasma membrane (37). VLDLR, as well as two other LDL receptor family members, LRP1b and Apoer2 (data not shown), was used as a negative control. Both LRP1 and Megf7 inhibited the Wnt-induced activation of the luciferase reporter to a similar extent in this assay (Fig. 9A), suggesting that Megf7, like LRP1, can also antagonize the LRP5/6-mediated activation of this signaling pathway. Neither VLDLR (Fig. 9A), nor LRP1b or Apoer2 (data not shown), had an effect on Wnt activity in this assay, indicating that inhibition of signaling by Megf7 was specific. Inhibition of Wnt signaling by Megf7 was dose-dependent (Fig. 9B). Increasing amounts of Megf7 progressively inhibited the Wnt1- and LRP6-dependent activation of the reporter.

DISCUSSION

*Megf*7/*Lrp*4 knockout mice were generated by homologous recombination. Homozygous knockout animals show fully penetrant polysyndactyly, sometimes combined with mild and only partially penetrant abnormalities of tooth development (Fig. 2). This striking phenotype first manifests itself at the early stages of limb bud development, when *Megf*7 is expressed in the AER, a stripe-shaped organizing center at the distal end of the limb bud and in the ventral ectoderm (Fig. 4). Loss of *Megf*7 results in disruption of the AER and ectopic expression of several genes required for laying down and maintaining the patterns that are required for the ordered development of the autopod. These genes encode signaling proteins of the *Fgf*, *Bmp* and *Shh* families, as well as several transcription factors that are also controlled by Wnt signals (Figs 5–8).

How does *Megf*7 regulate limb development? Although this initial study into the physiological role of *Megf*7 cannot provide a comprehensive answer to this complex and still incompletely understood process, the results of this study have nevertheless revealed a pivotal role for *Megf*7 in the regulation of essential signaling pathways that emanate from the AER and that act in a coordinated fashion to direct the proper development of the autopod. As a transmembrane protein and cell surface receptor, Megf7 could participate in this process in various ways for which precedents have emerged from studies on other members of the LDL receptor gene family.

LDL receptor family members can either signal directly or indirectly modulate the function of other primary signal transducers. For instance, Apoer2 and Vldlr can recruit and directly stimulate non-receptor tyrosine kinases of the Src family and other intracellular kinase cascades in response to Reelin binding to their extracellular domains (38–40). Another example is LRP1, which interacts with the PDGF receptor-β (PDGFRβ) and thereby modulates the subcellular trafficking of this receptor tyrosine kinase (41). However, LRP1 also serves as a co-receptor for PDGFRβ, inasmuch as its cytoplasmic domain undergoes tyrosine phosphorylation in response to PDGFRβ signaling (7,9), which can now act as a scaffold for the recruitment of other signal transducers, specifically the Shc adapter protein (42). This co-receptor function of LRP1 is of vital importance for the regulation of PDGF signaling and for the maintenance of the integrity of the vascular wall (6). Moreover, LRP1 has recently been suggested to function as a co-receptor for Frizzled-1, a receptor for Wnt3a (37). We have confirmed that LRP1 can negatively regulate Wnt signaling *in vitro* and that Megf7 can function in a similar manner (Fig. 9). LRP1 has also been recognized to be identical to the large TGFβ-receptor V (43), further supporting a multifunctional role of this versatile protein as a modulator of diverse signaling processes.

Megalin is another large member of the LDL receptor gene family that is involved in the regulation of a range of other

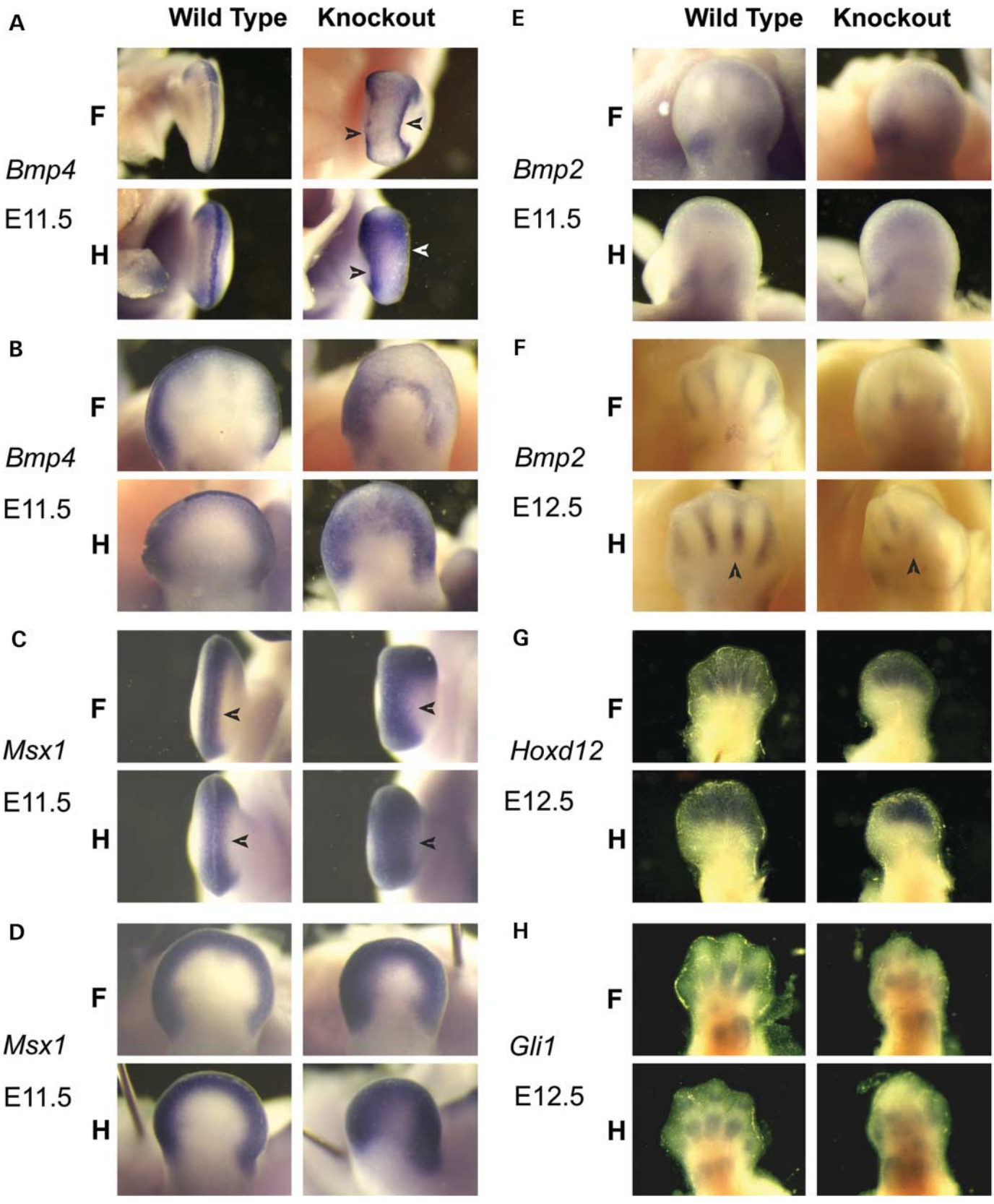

Figure 8. Whole mount *in situ* hybridization for *Msx*1, *Bmp*4, *Bmp*2, *Hoxd*12 and *Gli*1 in wild-type and knockout embryos. Expression of *Msx*1 at E11.5: (**A**) apical view and (**B**) lateral view. Expression of *Msx*1 at E11.5: (**C**) apical view and (**D**) lateral view. Expression of *Bmp*2 at E11.5 (**E**) and E12.5 (**F**). Expression of *Hoxd*12 (**G**) and *Gli*1 (**H**) at E12.5.

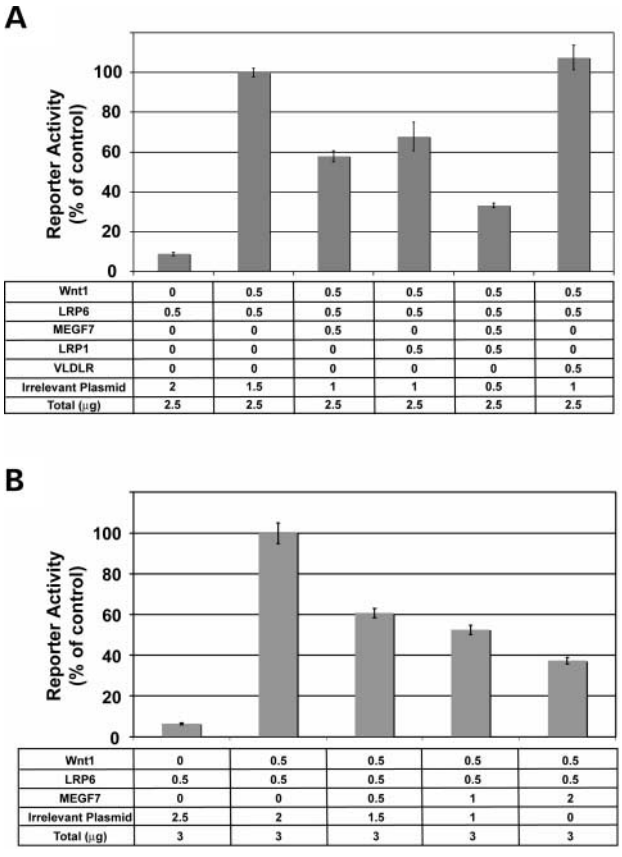

Wnt1	0	0.5	0.5	0.5	0.5	0.5
LRP6	0.5	0.5	0.5	0.5	0.5	0.5
MEGF7	0	0	0.5	0	0.5	0
LRP1	0	0	0	0.5	0.5	0
VLDLR	0	0	0	0	0	0.5
Irrelevant Plasmid	2	1.5	1	1	0.5	1
Total (μg)	2.5	2.5	2.5	2.5	2.5	2.5

Wnt1	0	0.5	0.5	0.5	0.5
LRP6	0.5	0.5	0.5	0.5	0.5
MEGF7	0	0	0.5	1	2
Irrelevant Plasmid	2.5	2	1.5	1	0
Total (μg)	3	3	3	3	3

Figure 9. Megf7 inhibits Wnt signaling *in vitro*. HEK-293 cells were transfected using the TOP-Flash reporter system as described in Materials and Methods in the presence of the indicated amounts of plasmids. (**A**) Megf7 and LRP1, but not VLDLR, inhibit Wnt signaling. Inhibition by co-transfection of Megf7 and LRP1 is additive. (**B**) Inhibition of Wnt signaling by Megf7 is dose-dependent. Increasing amounts of Megf7 plasmid (0.5–2 μg) were transfected together with constant amounts of LRP6 (an activating Wnt co-receptor) and Wnt1 (the activating ligand). All determinations were performed in triplicate. Between 3 and 11 independent determinations were performed for each condition. Error bars represent SEM ($P < 0.05$).

distinct cellular signaling pathways. It modulates the signaling of steroid hormones by mediating their intercellular transport and uptake. Notably, however, Megalin has been reported to bind Shh at its extracellular domain (44), as well as Bmps, specifically Bmp4. Loss of Megalin expression results in a patterning defect of the ventral telencephalon, which is caused by increased Bmp4 signaling and concomitant loss of Shh expression in the ventral forebrain. The mechanism by which Megalin deficiency causes this defect has been attributed to decreased clearance of Bmp4 (45).

The physiological consequences of the Megalin defect for brain development bear some resemblance to the ones we have uncovered here in the *Megf7* knockout for limb formation. However, the specific mechanism(s) that apply to *Megf7* in this case require a series of further extensive investigations. As has been suggested for Megalin, Megf7 might serve as a clearance receptor for signaling proteins that are secreted by the AER or surrounding tissues, including Bmps. A role for *Megf7* in tooth development (Fig. 2C), which also requires *Bmp receptor 1A* (23), is consistent with such a function. Another attractive mechanism by which *Megf7* might conceivably control AER formation and maintenance could involve a co-receptor function, similar to the one LRP1 plays in conjunction with PDGFRβ. Potential interacting partners include Fgf, Bmp and Frizzled receptors or the Shh signaling complex. It is also possible that Megf7, like Megalin or LRP1, can interact with more than one of these ligands or receptors, alone or in combination. A role of Megf7 in Wnt signaling is very likely, because of the strong resemblance of the *Megf7* knockout phenotype with the *doubleridge* mutation, which affects *Dkk1*, a negative regulator of Wnt signaling (20,21,46). This is also supported by the ability of Megf7 to potently antagonize canonical Wnt signaling through β-catenin in an *in vitro* reporter assay (Fig. 9). The striking expansion of the AER is consistent with abnormally increased Wnt signaling in the AER (19). However, inasmuch as *Megf7* can antagonize Lrp5/6-dependent activation of the canonical Wnt signaling pathway (Fig. 9), the current data cannot exclude a possible independent role for *Megf7* as a mediator of a non-canonical Wnt signal in lieu of *Lrp5/6*.

Megf7 does not appear to play a major role in establishing dorsal–ventral polarity, although the expansion of the AER results in the proximal displacement of the *Wnt7a* expression in the dorsal ectoderm (Supplementary Material, Fig. S3). However, the abnormal expansion of the AER in the *Megf7* knockouts appears symmetrical (Figs 4 and 5) and *Lmx1b* expression is only mildly affected in the mutants (Fig. 7).

The conclusive molecular dissection of the signaling pathways that are modulated by *Megf7* is not a straightforward process, because these pathways themselves are often regulated by accessory proteins—such as Megf7, or other adaptor or scaffolding proteins—in a cell-type-specific fashion. A detailed understanding of the molecular mechanisms by which *Megf7* regulates the complex processes that culminate in the formation of the distal limbs will require the use of a battery of experimental systems *in vitro* and *in vivo* that are best adapted to the study of the diverse signaling pathways in which *Megf7* could be involved, as well as the generation and analysis of a series of compound mutant strains of mice that carry specific mutations in *Megf7* or putative interacting proteins. Our current findings establish a physiological role for *Megf7*, which, like other members of the LDL receptor gene family, can function as modulator and potentially as an integrator of diverse signaling pathways during development.

MATERIALS AND METHODS

Generation of *Megf7* knockout mice

A replacement-type vector was constructed using long and short arms of homology amplified by PCR from ES cell genomic DNA using long-range PCR (Takara Biochemical, Inc., Berkeley, CA) and the following primers: KI3 (5′-CCA CCACCTGCAGGGTATACTGAGGAGTCCACCGATGGCA TAGCTG-3′) and KI4 (5′-CCACCACCTGCAGGCGGCCG CGAATATGATATCATGTCAATACTAGAGACTTACC-3′) were used as 5′ and 3′ primers, respectively, to amplify the long arm. MEJ76 (5′-CCACCACTCGAGCCTGTGGACCT TCCTAT AAGTCAACTTCC 3′) and MEJ77 (5′-CCACCA

CTCGAGGGTTGACTGCTAACAATCAGAGCAGGCTG-3′) were used as 5′ and 3′ primers, respectively, for the short arm. The short arm was cloned into pJB1 (47) at the *Xho*I site. The long arm was mutated using MEJ143 (5′-CCTAGGTGAAGG ACTGTAAGTCAGCTATGCCATC-3′) and MEJ144 (5′-GATGGCATAGCTGACTTACAGTCCTTCACCTAGG-3′) to introduce a stop codon into exon 36. The mutated long arm and the bovine growth hormone 3′ untranslated region were cloned into the pJB1-short arm containing plasmid using *Not*I to generate the targeting vector. Recombinant ES cell clones were generated by electroporating the linearized vector into SM1 ES cells. Clones were selected by PCR, verified by Southern blotting and two independent *Megf*7 knockout strains of mice were generated by crossing chimeric male mice with C57BL/6 females as previously described (48). All subsequent analyses were done on a 129SvEv × C57BL/6 hybrid background.

Mice were genotyped by PCR as follows: MEJ155 (5′-CCC AGCTGGGCCTCTGTGCACATTCCAATG-3′) and MEJ166 (5′-CCATGGCCTCTGCATTAGTTCTTGCTCTC-3′) were used to selectively amplify the wild-type allele and MEJ156 (5′-CTCTGAAAGGGATGCCCAGCTGGGCCTCTG-3′) and MEJ267 (5′ CGATGGCATAGCTGACTTA-3′) were used to amplify the knockout allele.

Southern blotting for detecting the 7.4 kb wild-type and the 4.5 kb knockout alleles was performed using standard techniques. The Southern probe was amplified by PCR from mouse genomic DNA using the following primers. MEJ150 (5′-GGC ACATATCCCAGCACACATAGAGGTCAG-3′) and MEJ151 (5′-AGTTTGCCCACACTATAAGACTCCTCAC-3′).

The fragment was labeled with P^{32}-dCTP using the Rediprime II kit (Amersham Pharmacia Biotech). ES cells were cultured without a feeder layer until they were almost confluent. Genomic DNA was isolated from the ES cells using proteinase K digestion and phenol/chloroform extraction. The isolated DNA was digested with *Eco*RI and *Sac*I, run on agarose gels and blotted onto Hybond-XL (Amersham Pharmacia Biotech). The labeled probe was hybridized to the membrane in Rapid-Hyb Buffer (Amersham Pharmacia Biotech) and washed. Bound radioactivity was detected by phosphoimager.

Alcian Blue/Alizarin Red staining

Adult and embryo skeletons were prepared and stained as previously described (49). Briefly, most of the soft tissue was removed from the adult mice and the skin and internal organs were removed from the P0 pups. Skeletons were fixed in ethanol. The lipids remaining on the skeletons were removed with acetone. Skeletons were then stained with Alizarin Red and Alcian Blue. The soft tissue was dissolved with potassium hydroxide and then clarified with glycerol.

Whole mount *in situ* hybridization

Whole mount *in situ* hybridization was performed as described previously but with a few minor modifications as described in (50). Briefly, embryos were harvested and fixed in 4% paraformaldehyde in PBS at 4°C. Fixed embryos were dehydrated through successive washes in methanol/PBST and stored at −20°C in methanol. Embryos were bleached in 6% hydrogen peroxide for 4–6 h at 22°C and then rehydrated through successive washes in methanol/PBST. Embryos were digested using 10 μg/ml proteinase K in PBST for varying times depending on the age and size of the specimen. The digest was quenched with two washes of 2 mg/ml glycine/PBST. Embryos were refixed in 0.2% glutaraldehyde, 4% paraformaldehyde, PBST for 20 min at 22°C. Embryos were incubated at 65°C in hybridization buffer (50% formamide, 5× SSC, 50 μg/ml tRNA, 0.05% heparin, 1% SDS) for 1 h followed by an overnight incubation at 65°C with the respective digoxigenin-UTP labeled probes. Embryos were then washed twice in wash buffer 1 (50% formamide, 5× SSC, 1% SDS) at 65°C, next with a 1:1 mix of wash buffer 1 and wash buffer 2 (0.5 M NaCl, 10 mM Tris, pH 7.4, 0.1% Tween-20) at 65°C, then in wash buffer 2 at 22°C (30 min per wash). Embryos were then treated with 100 μg/ml RNase A in wash buffer 2 for 30 min at 37°C, followed by two incubations in wash buffer 3 (50% formamide, 2× SSC, 0.1% Tween-20) for 30 min at 65°C. Embryos were then rinsed in TBST and treated with Blocking Solution (TBST containing 10% sheep serum, 2% BSA, 2 mM levamisole) for 1 h before incubation overnight at 4°C in the alkaline phosphatase-coupled anti-digoxigenin antibody-containing solution [TBST, 1% sheep serum, 2% BSA, 2 mM levamisole, 1:2000 anti-dig-AP (from Roche Applied Science)]. Embryos were washed several times in TBST containing 2 mM levamisole. Color reaction was developed in NTMT with 0.34 mg/ml NBT and 0.18 mg/ml BCIP, and embryos were washed in TBST, dehydrated and rehydrated with successive washes of TBST/methanol. For sectioning, stained embryos were washed three times in PBS and embedded in 2% agarose. Fifty-to-hundred micrometer-serial sections were obtained using a VT1000S vibratome (Leica).

To reduce the number of animals used in these experiments and to facilitate analysis, both wild-type and heterozygous embryos were used as controls and designated wild-type, as they were phenotypically indistinguishable, and compared with homozygous littermate embryos. Probes were generated from reverse-transcribed RNA using the following primers. Megf7: MEJ354 (5′-ggcctgtgcatcaactcgggctggcgctg-3′) and MEJ355 (5′-ctggaaagccccttcagtgtttgtgcagccc-3′); Fgf8: MEJ173 (5′-gagagatctagaTGGAGACCGATACTTTTGGAA GCAGAGTC-3′) and MEJ174 (5′-ccaattactagtgcaaacaatatgca caactagaaggcagctccc-3′); *Col2a*1: MEJ330 (5′-CCAATGATG TAGAGATGAGGGCCGAGGGCAAC-3′) and MEJ331 (5′-GATGTTTTAAAAAATACAGAGGTGTTTGAC-3′); Lmx1b: MEJ322 (5′-TGAAGAGTGAGGATGAAGATGGAGACA TG-3′) and MEJ323 (5′-GGAGGCAAAGTAGGAGCTC TGCATGGAGTAG-3′); Hoxd12: MEJ328 (5′-TCTACTTTT CCAACCTGAGAGCCAATGGCAG-3′) and MEJ329 (5′-TT GTGTAGGGTTTCCTCTTCTTGCGGGCCC-3′); Bmp2: MEJ324 (5′-GTGGCCGGGACCCGCTGTCTTCTAGTGTT G-3′) and MEJ325 (5′-GGTGACGTCGAAGCTCTCCCACT GACTTGTG-3′); Gli1: MEJ326 (5′-GAAACTTTCACCGT GGGGGTAAACAGGCCTTC-3′) and MEJ327 (5′-CCTTTAT TGTCAGGAAACTGTGCTATTATTAAAG-3′). *Shh*, *Msx*1 and *Bmp*4 probes were kindly provided by Deepak Srivastava, Gladstone Institutes, UCSF, San Francisco, CA, USA (51,52).

Whole mount TUNEL assay

Embryos were prepared and stored in pre-hybridization buffer at −20°C as described in the whole mount *in situ* methods. Embryos were then thoroughly washed overnight in PBS and equilibrated in 100 μl TUNEL Label mix (Roche Applied Science) at room temperature for 5 min. The TUNEL Label mix was replaced with 95 μl TUNEL Label mix and 5 μl TUNEL Enzyme and incubated at 37°C for 2 h. Embryos were then washed in TBST and labeled using TUNEL AP antibody at 100 μl/embryo and stained as described earlier for the whole mount *in situ* hybridizations.

Wnt activity assay

HEK-293 cells were plated at 400 000 cells/well in 6-well plates and grown to 50–80% confluency in 10% FBS/DMEM. Cells were transfected using the TOP-Flash reporter system (Upstate Cell Signaling Solutions) and the indicated expression plasmids for Wnt1, LRP6, Megf7, LRP1 and VLDLR in pCDNA3.1. Transfections were performed with the Fugene 6 reagent (Roche) using the manufacturer's protocol. Cells were lysed 2 days after transfection and lysates were assayed for firefly and runilla luciferase activities using the Dual Luciferase Reporter Assay System (Promega). Transfections were performed in triplicate. Each transfection was measured in triplicate. Between 3 and 11 independent samples were assayed for each condition.

SUPPLEMENTARY MATERIAL

Supplementary Material is available at HMG Online.

ACKNOWLEDGEMENTS

We are indebted to Wen-Ling Niu, Huichuan Reyna, Karen Brown, Debbie Morgan, Priscilla Rodriguez, Isaac Rocha and Elizabeth Lummus for excellent technical assistance and to Keith Wharton for discussions and helpful comments. This work was supported by National Institutes of Health (NIH) Grants HL20948, HL63762 and NS43408, the Alzheimer's Association, the Wolfgang-Paul Award of the Humboldt Foundation and the Perot Family Foundation.

Conflicts of Interest statement. The authors declare no conflicts of interest.

REFERENCES

1. Nakayama, M., Nakajima, D., Nagase, T., Nomura, N., Seki, N. and Ohara, O. (1998) Identification of high-molecular-weight proteins with multiple EGF-like motifs by motif-trap screening. *Genomics*, **51**, 27–34.
2. Herz, J. and Bock, H.H. (2002) Lipoprotein receptors in the nervous system. *Annu. Rev. Biochem.*, **71**, 405–434.
3. Trommsdorff, M., Gotthardt, M., Hiesberger, T., Shelton, J., Stockinger, W., Nimpf, J., Hammer, R.E., Richardson, J.A. and Herz, J. (1999) Reeler/disabled-like disruption of neuronal migration in knockout mice lacking the VLDL receptor and ApoE receptor 2. *Cell*, **97**, 689–701.
4. Beffert, U., Weeber, E.J., Durudas, A., Qiu, S., Masiulis, I., Sweatt, J.D., Li, W.-P., Adelmann, G., Frotscher, M., Hammer, R.E. *et al.* (2005) Modulation of synaptic plasticity and memory by Reelin involves differential splicing of the lipoprotein receptor Apoer2. *Neuron*, **47**, 567–579.
5. Herz, J. and Strickland, D.K. (2001) LRP: a multifunctional scavenger and signaling receptor. *J. Clin. Invest.*, **108**, 779–784.
6. Boucher, P., Gotthardt, M., Li, W.P., Anderson, R.G. and Herz, J. (2003) LRP: role in vascular wall integrity and protection from atherosclerosis. *Science*, **300**, 329–332.
7. Boucher, P., Liu, P., Gotthardt, M., Hiesberger, T., Anderson, R.G. and Herz, J. (2002) Platelet-derived growth factor mediates tyrosine phosphorylation of the cytoplasmic domain of the low density lipoprotein receptor-related protein in caveolae. *J. Biol. Chem.*, **277**, 15507–15513.
8. Herz, J. and Hui, D.Y. (2004) Lipoprotein receptors in the vascular wall. *Curr. Opin. Lipidol.*, **15**, 175–181.
9. Loukinova, E., Ranganathan, S., Kuznetsov, S., Gorlatova, N., Migliorini, M.M., Loukinov, D., Ulery, P.G., Mikhailenko, I., Lawrence, D.A. and Strickland, D.K. (2002) Platelet-derived growth factor (PDGF)-induced tyrosine phosphorylation of the low density lipoprotein receptor-related protein (LRP): evidence for integrated co-receptor function between LRP and the PDGF. *J. Biol. Chem.*, **277**, 15499–15506.
10. Chen, W.J., Goldstein, J.L. and Brown, M.S. (1990) NPXY, a sequence often found in cytoplasmic tails, is required for coated pit-mediated internalization of the low density lipoprotein receptor. *J. Biol. Chem.*, **265**, 3116–3123.
11. Gotthardt, M., Trommsdorff, M., Nevitt, M.F., Shelton, J., Richardson, J.A., Stockinger, W., Nimpf, J. and Herz, J. (2000) Interactions of the low density lipoprotein receptor gene family with cytosolic adaptor and scaffold proteins suggest diverse biological functions in cellular communication and signal transduction. *J. Biol. Chem.*, **275**, 25616–25624.
12. Nykjaer, A. and Willnow, T.E. (2002) The low-density lipoprotein receptor gene family: a cellular Swiss army knife? *Trends Cell. Biol.*, **12**, 273–280.
13. Pinson, K.I., Brennan, J., Monkley, S., Avery, B.J. and Skarnes, W.C. (2000) An LDL-receptor-related protein mediates Wnt signalling in mice. *Nature*, **407**, 535–538.
14. Tamai, K., Semenov, M., Kato, Y., Spokony, R., Liu, C., Katsuyama, Y., Hess, F., Saint-Jeannet, J.P. and He, X. (2000) LDL-receptor-related proteins in Wnt signal transduction. *Nature*, **407**, 530–535.
15. Wehrli, M., Dougan, S.T., Caldwell, K., O'Keefe, L., Schwartz, S., Vaizel-Ohayon, D., Schejter, E., Tomlinson, A. and DiNardo, S. (2000) Arrow encodes an LDL-receptor-related protein essential for Wingless signalling. *Nature*, **407**, 527–530.
16. Capdevila, J. and Izpisua Belmonte, J.C. (2001) Patterning mechanisms controlling vertebrate limb development. *Annu. Rev. Cell Dev. Biol.*, **17**, 87–132.
17. Logan, C., Hornbruch, A., Campbell, I. and Lumsden, A. (1997) The role of Engrailed in establishing the dorsoventral axis of the chick limb. *Development*, **124**, 2317–2324.
18. Barrow, J.R., Thomas, K.R., Boussadia-Zahui, O., Moore, R., Kemler, R., Capecchi, M.R. and McMahon, A.P. (2003) Ectodermal Wnt3/beta-catenin signaling is required for the establishment and maintenance of the apical ectodermal ridge. *Genes Dev.*, **17**, 394–409.
19. Soshnikova, N., Zechner, D., Huelsken, J., Mishina, Y., Behringer, R.R., Taketo, M.M., Crenshaw, E.B., III and Birchmeier, W. (2003) Genetic interaction between Wnt/beta-catenin and BMP receptor signaling during formation of the AER and the dorsal–ventral axis in the limb. *Genes Dev.*, **17**, 1963–1968.
20. Adamska, M., MacDonald, B.T. and Meisler, M.H. (2003) Doubleridge, a mouse mutant with defective compaction of the apical ectodermal ridge and normal dorsal–ventral patterning of the limb. *Dev. Biol.*, **255**, 350–362.
21. Adamska, M., MacDonald, B.T., Sarmast, Z.H., Oliver, E.R. and Meisler, M.H. (2004) En1 and Wnt7a interact with Dkk1 during limb development in the mouse. *Dev. Biol.*, **272**, 134–144.
22. Miyazono, K., Kusanagi, K. and Inoue, H. (2001) Divergence and convergence of TGF-beta/BMP signaling. *J. Cell. Physiol.*, **187**, 265–276.
23. Andl, T., Ahn, K., Kairo, A., Chu, E.Y., Wine-Lee, L., Reddy, S.T., Croft, N.J., Cebra-Thomas, J.A., Metzger, D., Chambon, P. *et al.* (2004) Epithelial Bmpr1a regulates differentiation and proliferation in postnatal hair follicles and is essential for tooth development. *Development*, **131**, 2257–2268.
24. Albrecht, A.N., Schwabe, G.C., Stricker, S., Boddrich, A., Wanker, E.E. and Mundlos, S. (2002) The synpolydactyly homolog (spdh) mutation in the mouse—a defect in patterning and growth of limb cartilage elements. *Mech. Dev.*, **112**, 53–67.

25. Riddle, R.D., Ensini, M., Nelson, C., Tsuchida, T., Jessell, T.M. and Tabin, C. (1995) Induction of the LIM homeobox gene Lmx1 by WNT7a establishes dorsoventral pattern in the vertebrate limb. *Cell*, **83**, 631–640.
26. Akita, K., Francis-West, P. and Vargesson, N. (1996) The ectodermal control in chick limb development: Wnt-7a, Shh, Bmp-2 and Bmp-4 expression and the effect of FGF-4 on gene expression. *Mech. Dev.*, **60**, 127–137.
27. Laufer, E., Dahn, R., Orozco, O.E., Yeo, C.Y., Pisenti, J., Henrique, D., Abbott, U.K., Fallon, J.F. and Tabin, C. (1997) Expression of radical fringe in limb-bud ectoderm regulates apical ectodermal ridge formation. *Nature*, **386**, 366–373.
28. Pizette, S. and Niswander, L. (1999) BMPs negatively regulate structure and function of the limb apical ectodermal ridge. *Development*, **126**, 883–894.
29. Selever, J., Liu, W., Lu, M.F., Behringer, R.R. and Martin, J.F. (2004) Bmp4 in limb bud mesoderm regulates digit pattern by controlling AER development. *Dev. Biol.*, **276**, 268–279.
30. Yang, Y. and Niswander, L. (1995) Interaction between the signaling molecules WNT7a and SHH during vertebrate limb development: dorsal signals regulate anteroposterior patterning. *Cell*, **80**, 939–947.
31. Parr, B.A. and McMahon, A.P. (1995) Dorsalizing signal Wnt-7a required for normal polarity of D–V and A–P axes of mouse limb. *Nature*, **374**, 350–353.
32. Loomis, C.A., Harris, E., Michaud, J., Wurst, W., Hanks, M. and Joyner, A.L. (1996) The mouse Engrailed-1 gene and ventral limb patterning. *Nature*, **382**, 360–363.
33. Zhang, Y., Zhang, Z., Zhao, X., Yu, X., Hu, Y., Geronimo, B., Fromm, S.H. and Chen, Y.P. (2000) A new function of BMP4: dual role for BMP4 in regulation of Sonic hedgehog expression in the mouse tooth germ. *Development*, **127**, 1431–1443.
34. Drossopoulou, G., Lewis, K.E., Sanz-Ezquerro, J.J., Nikbakht, N., McMahon, A.P., Hofmann, C. and Tickle, C. (2000) A model for anteroposterior patterning of the vertebrate limb based on sequential long- and short-range Shh signalling and Bmp signalling. *Development*, **127**, 1337–1348.
35. Stott, N.S., Jiang, T.X. and Chuong, C.M. (1999) Successive formative stages of precartilaginous mesenchymal condensations *in vitro*: modulation of cell adhesion by Wnt-7A and BMP-2. *J. Cell. Physiol.*, **180**, 314–324.
36. Mariani, F.V. and Martin, G.R. (2003) Deciphering skeletal patterning: clues from the limb. *Nature*, **423**, 319–325.
37. Zilberberg, A., Yaniv, A. and Gazit, A. (2004) The low density lipoprotein receptor-1, LRP1, interacts with the human frizzled-1 (HFz1) and down-regulates the canonical Wnt signaling pathway. *J. Biol. Chem.*, **279**, 17535–17542.
38. Arnaud, L., Ballif, B.A., Forster, E. and Cooper, J.A. (2003) Fyn tyrosine kinase is a critical regulator of disabled-1 during brain development. *Curr. Biol.*, **13**, 9–17.
39. Bock, H.H. and Herz, J. (2003) Reelin activates SRC family tyrosine kinases in neurons. *Curr. Biol.*, **13**, 18–26.
40. Bock, H.H., Jossin, Y., Liu, P., Forster, E., May, P., Goffinet, A.M. and Herz, J. (2003) Phosphatidylinositol 3-kinase interacts with the adaptor protein Dab1 in response to Reelin signaling and is required for normal cortical lamination. *J. Biol. Chem.*, **278**, 38772–38779.
41. Takayama, Y., May, P., Anderson, R.G. and Herz, J. (2005) Low density lipoprotein receptor-related protein 1 (LRP1) controls endocytosis and c-CBL-mediated ubiquitination of the platelet-derived growth factor receptor beta (PDGFRbeta). *J. Biol. Chem.*, **280**, 18504–18510.
42. Barnes, H., Larsen, B., Tyers, M. and van Der Geer, P. (2001) Tyrosine-phosphorylated low density lipoprotein receptor-related protein 1 (Lrp1) associates with the adaptor protein SHC in SRC-transformed cells. *J. Biol. Chem.*, **276**, 19119–19125.
43. Huang, S.S., Ling, T.Y., Tseng, W.F., Huang, Y.H., Tang, F.M., Leal, S.M. and Huang, J.S. (2003) Cellular growth inhibition by IGFBP-3 and TGF-beta1 requires LRP-1. *FASEB J.*, **17**, 2068–2081.
44. McCarthy, R.A., Barth, J.L., Chintalapudi, M.R., Knaak, C. and Argraves, W.S. (2002) Megalin functions as an endocytic sonic hedgehog receptor. *J. Biol. Chem.*, **277**, 25660–25667.
45. Spoelgen, R., Hammes, A., Anzenberger, U., Zechner, D., Andersen, O.M., Jerchow, B. and Willnow, T.E. (2005) LRP2/megalin is required for patterning of the ventral telencephalon. *Development*, **132**, 405–414.
46. Adamska, M., Billi, A.C., Cheek, S. and Meisler, M.H. (2005) Genetic interaction between Wnt7a and Lrp6 during patterning of dorsal and posterior structures of the mouse limb. *Dev. Dyn.*, **233**, 368–372.
47. Gotthardt, M., Hammer, R.E., Hubner, N., Monti, J., Witt, C.C., McNabb, M., Richardson, J.A., Granzier, H., Labeit, S. and Herz, J. (2003) Conditional expression of mutant M-line titins results in cardiomyopathy with altered sarcomere structure. *J. Biol. Chem.*, **278**, 6059–6065.
48. Willnow, T.E. and Herz, J. (1994) Homologous recombination for gene replacement in mouse cell lines. *Meth. Cell Biol.*, **43**, 305–334.
49. McLeod, M.J. (1980) Differential staining of cartilage and bone in whole mouse fetuses by Alcian Blue and Alizarin Red S. *Teratology*, **22**, 299–301.
50. Hogan, B., Beddington, R., Constantini, F. and Lacy, E. (1994) *Manipulating the Mouse Embryo*. 2nd ed. Cold Spring Harbor Laboratory Press, Cold Spring Harbor, New York.
51. Fernandez-Teran, M., Piedra, M.E., Kathiriya, I.S., Srivastava, D., Rodriguez-Rey, J.C. and Ros, M.A. (2000) Role of dHAND in the anterior–posterior polarization of the limb bud: implications for the Sonic hedgehog pathway. *Development*, **127**, 2133–2142.
52. Thomas, T., Kurihara, H., Yamagishi, H., Kurihara, Y., Yazaki, Y., Olson, E.N. and Srivastava, D. (1998) A signaling cascade involving endothelin-1, dHAND and msx1 regulates development of neural-crest-derived branchial arch mesenchyme. *Development*, **125**, 3005–3014.